



Short communication

The effect of oxygen vacancies on the structure and electrochemistry of $\text{LiTi}_2(\text{PO}_4)_3$ for lithium-ion batteries: A combined experimental and theoretical study

Jia-Yan Luo^a, Li-Juan Chen^b, Yu-Jun Zhao^b, Ping He^a, Yong-Yao Xia^{a,*}

^a Department of Chemistry and Shanghai Key Laboratory of Molecular Catalysis and Innovative Materials, Institute of New Energy, Fudan University, Handan Road 220, Shanghai 200433, PR China

^b Department of Physics, South China University of Technology, Guangzhou 510640, PR China

ARTICLE INFO

Article history:

Received 9 March 2009

Received in revised form 9 June 2009

Accepted 15 June 2009

Available online 24 June 2009

Keywords:

First-principles calculations

Conductivity

Rate capability

XPS

Nasicon

VASP

ABSTRACT

We report that a partially oxygen deficient $\text{LiTi}_2(\text{PO}_4)_3$ shows a much better rate capability as a cathode material for lithium-ion batteries compared to stoichiometric $\text{LiTi}_2(\text{PO}_4)_3$. A combination of X-ray diffraction (XRD), X-ray photoelectron spectroscopy (XPS), electrochemistry, and first-principles calculations was used to determine and rationalize the structural and electrical changes that occur with different heat treatment atmospheres. XRD and XPS experiments confirmed that some Ti^{4+} transformed to Ti^{3+} in oxygen deficient $\text{LiTi}_2(\text{PO}_4)_3$ heat treated under N_2 ; Ti^{3+} was detected and the lattice parameter increased compared to that of $\text{LiTi}_2(\text{PO}_4)_3$. Electrical conductivity measurements indicated an increase in the electronic conductivity of nearly two orders of magnitude for the oxygen deficient $\text{LiTi}_2(\text{PO}_4)_3$ sample compared to $\text{LiTi}_2(\text{PO}_4)_3$. First-principles calculations suggest that the oxygen vacancies could be formed in $\text{LiTi}_2(\text{PO}_4)_3$ under oxygen-poor conditions, and this may significantly decrease the donor levels of other possible donor defects and thus improve the electronic mobility.

© 2009 Elsevier B.V. All rights reserved.

1. Introduction

Lithium-ion batteries are often used in everyday life, especially in consumer electronic devices such as cellular phones, notebook computers, compact camcorders, and electric vehicles (EVs)/hybrid electric vehicles (HEVs). The cost, safety, environmental friendliness, and long operational life of the cathode materials are of major concern for applications of large-scale lithium-ion batteries [1–3]. Cobalt oxide-based materials are unsafe and environmentally hazardous. Manganese-based materials are attractive because of both their low cost and low toxicity. However, they suffer from capacity fading during cycling, especially at high temperatures [4–5].

Since Goodenough and co-workers [6,7] reported that a new generation of electrode materials based on 3-D phosphate opened-frameworks could reversibly insert lithium, tremendous effort has been devoted to improving the performance of these compounds. They have high lithium-ion mobility and better thermal properties than conventional cathode materials, and they benefit from the inductive effect generated by the polyanionic groups, which lowers the energy of the transition metal redox couple in the phosphate-based electrode materials with respect to the Fermi

level of lithium [8–10]. However, the disadvantages, including low electronic conductivity, prevent them from being widely used in large-scale applications.

Consequently, several approaches have been developed to overcome this problem. One is to develop nanostructured electrode materials: nanosized particles can reduce the lithium-ion diffusion path, thus improving the rate capability, as well as providing a large contact surface area with the electrolyte and electronic conductive material. However, such an improvement is often achieved at the expense of high volumetric energy density [11–20]. Another way is to reduce the electrode polarization by improving its electrical conductivity, which often involves modifying electrode materials through surface carbon-coating. This treatment process actually works because the coated carbon layer can greatly reduce the electrode conductivity resistance by creating a close-to-optimal wiring situation for the conduction of electrons, which is much better than mixing electrode-conductive materials such as carbon black (CB) with the active electrode materials [20–23]. For example, we have recently shown that about 80% of the reversible capacity of carbon-coated $\text{LiTi}_2(\text{PO}_4)_3$ at a rate of 0.1 C could be obtained even at a rate of 10 C [24], which is much higher than the previous result that only 77% of the reversible capacity was delivered at 2 C [25]. Similar improvement has also been widely reported for other electrode materials, especially LiFePO_4 and $\text{Li}_4\text{Ti}_5\text{O}_{12}$ [26–35]. However, beyond the surface coated carbon, how do the heat treatment

* Corresponding author. Tel.: +86 21 55664177; fax: +86 21 55664177.
E-mail address: yyxia@fudan.edu.cn (Y.-Y. Xia).

atmospheres influence the structural change and electrical conductivity of bulk electrode materials, such as $\text{LiTi}_2(\text{PO}_4)_3$, LiFePO_4 and $\text{Li}_4\text{Ti}_5\text{O}_{12}$? There have been few systematic studies and a lack of understanding on how the structural defects, electrical conductivity and rate capability are influenced by the different heat treatment atmospheres of the electrode materials.

Herein, we systematically studied for the first time the effects of heat treatment atmospheres on the electrochemical properties of $\text{LiTi}_2(\text{PO}_4)_3$ electrodes by means of the charge/discharge test, X-ray diffraction (XRD) and X-ray photoelectron spectroscopy (XPS) analyses, and *ab initio* studies. The structural and electronic properties of $\text{LiTi}_2(\text{PO}_4)_3$ compounds were extracted from first-principles calculations as well. Such analyses regarding battery materials have been performed in the past using the total or difference charge density and the electronic density of states [36–38].

2. Methodology

2.1. Experiment

$\text{LiTi}_2(\text{PO}_4)_3$ was synthesized using a conventional solid-state reaction. Stoichiometric amounts of Li_2CO_3 , $(\text{NH}_4)_2\text{H}_2\text{PO}_4$ and TiO_2 were mixed and homogenized in a mortar and slowly heated to 1000°C , and then annealed at that temperature for 48 h in air. For the oxygen deficient $\text{LiTi}_2(\text{PO}_4)_3$, the as prepared $\text{LiTi}_2(\text{PO}_4)_3$ powder was transferred into a reaction tube with nitrogen gas flow through the reaction tube at a rate of 1 L min^{-1} . The reaction temperature was maintained at 900°C for 12 h.

Powder XRD measurements were performed on a Rigaku D/MAX-IIA X-ray diffractometer using $\text{Cu K}\alpha$ radiation. The chemical states of the surfaces of the samples were investigated by XPS with a Thermo ESCALAB 250 XPS spectrometer at a pass energy of 50 eV (0.1 eV/step), using $\text{Al K}\alpha$ as the exciting X-ray source. The spectra were calibrated with respect to the C 1s peak resulting from the adventitious hydrocarbon, which has an energy of 284.6 eV.

The *dc* electrical conductivity was measured by a direct volt-ampere method on disk samples prepared by pressing the powder up to 20 MPa, which ensures that the conductivity reaches a stable value. Their diameter and thickness were 1.2 cm and 1 mm, respectively. Electrical conductivity measurements were carried on a Solartron Instruments model 1287 electrochemical interface controlled by a computer.

Electrochemical measurements were carried out in a CR2016-type coin cell with lithium metal as the negative electrode. The working electrode was fabricated by compressing a mixture of the active materials, the conductive material (acetylene black (AB)), and the binder (polytetrafluoroethylene (PTFE)) in a weight ratio of $\text{LiTi}_2(\text{PO}_4)_3/\text{AB}/\text{PTFE} = 85:10:5$ onto an aluminum grid at 10 MPa. The electrodes were punched in the form of disks, typically with a diameter of 12 mm and a weight of about 10 mg, and then dried at 120°C for 12 h. The cell assembly was operated in a glove box filled with pure argon. The electrolyte solution was 1 M LiPF_6 /ethylene carbonate (EC)/propylene carbonate (PC)/diethyl carbonate (DEC) at a ratio of 1:1:1 by volume. The cell was galvanostatically cycled between 1.5 and 3.5 V vs. Li/Li^+ at various current densities at 25°C . Lithium insertion into the $\text{LiTi}_2(\text{PO}_4)_3$ electrode was referred to as discharge and extraction as charge.

2.2. Computation

All the calculations were done according to the pseudopotential plane wave method within the generalized gradient approximation of PW91 formulae [39], and the projector augmented wave (PAW) potentials, as implemented by the VASP code [40,41]. The possible oxygen defects were simulated by removing a single O

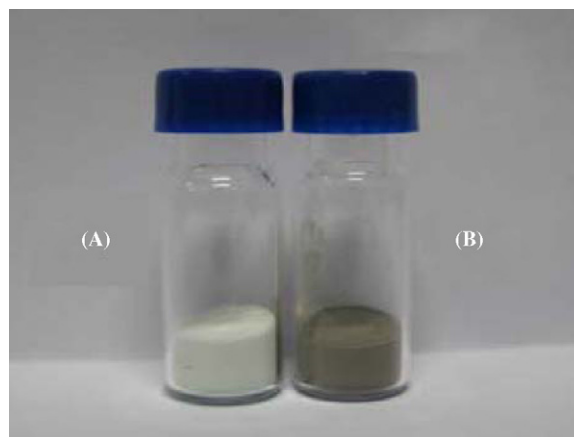


Fig. 1. Photographs of the $\text{LiTi}_2(\text{PO}_4)_3$ samples heat treated (A) under air and (B) under N_2 .

atom in a 108-atom $\text{LiTi}_2(\text{PO}_4)_3$ supercell. The charge density was obtained from the Monkhorst-Pack \mathbf{k} -space integration method, using the Γ -centered $2 \times 2 \times 1$ mesh, while a Γ -centered $4 \times 4 \times 2$ mesh was adopted for the final density of states. An energy cut-off of 400.0 eV was used for the plane wave basis expansion. The formation enthalpy for oxygen vacancy defects was calculated with the well-established formalism [42]:

$$\Delta H_f^{(\alpha,q)} = E(\alpha, q) - E(0) + \sum_{\alpha} n_{\alpha} (\Delta u_{\alpha} + u_{\alpha}^{\text{Solid}}) + q(E_{\text{VBM}} + E_F) \quad (1)$$

where $E(\alpha, q)$ and $E(0)$ are the total energy of the supercell with and without defect α . Here, $(\Delta u_{\alpha} + u_{\alpha}^{\text{Solid}})$ is the absolute value of the chemical potential of atom α , and n_{α} is the number of atoms for each defect; $n_{\alpha} = -1$ if an atom is added, while $n_{\alpha} = 1$ if an atom is removed. E_{VBM} represents the energy of the VBM of the defect-free system, and E_F is the Fermi energy relative to the E_{VBM} . The atomic structure was fully relaxed in our calculation. q is the valence state.

3. Results and discussion

Fig. 1 compares the color of the $\text{LiTi}_2(\text{PO}_4)_3$ sample with that of the sample heat treated under N_2 . It can be seen clearly that the $\text{LiTi}_2(\text{PO}_4)_3$ sample is white in color, which is consistent with previous results [25,35,43]. However, the sample heat treated under N_2 is gray. A similar phenomenon was found in a report on $\text{Li}_4\text{Ti}_5\text{O}_{12}$: the $\text{Li}_4\text{Ti}_5\text{O}_{12}$ sample heated under air was white, whereas the sample heated under H_2/Ar was gray due to the presence of the mixed $\text{Ti}^{4+}/\text{Ti}^{3+}$ valence in the sample [44].

The X-ray diffraction (XRD) patterns of the Nasicon $\text{LiTi}_2(\text{PO}_4)_3$ and oxygen deficient $\text{LiTi}_2(\text{PO}_4)_3$ are shown in Fig. 2. Graphite was added into the samples for calibration. Both of the samples, $\text{LiTi}_2(\text{PO}_4)_3$ prepared under air and oxygen deficient $\text{LiTi}_2(\text{PO}_4)_3$ prepared under N_2 , were phase-pure according to their XRD patterns. All the diffraction peaks of both patterns can be indexed in the rhombohedral crystal system (space group R3c). These results agree reasonably well with previous crystallographic data for this compound [25,35]. The only difference between the two XRD patterns is tailing the diffraction peaks to lower 2θ values for the oxygen deficient $\text{LiTi}_2(\text{PO}_4)_3$ sample heated under N_2 compared to the $\text{LiTi}_2(\text{PO}_4)_3$ under air. The tailing may originate from incomplete reduction of their sample because inner part of each particle is not reduced. The lattice parameter of $\text{LiTi}_2(\text{PO}_4)_3$, determined from Rietveld analysis of the XRD pattern, is $a \sim 8.497 \text{ \AA}$ and $c \sim 20.819 \text{ \AA}$. The lattice parameter $a \sim 8.508 \text{ \AA}$ and $c \sim 20.833 \text{ \AA}$ of oxygen deficient $\text{LiTi}_2(\text{PO}_4)_3$ is slightly larger than that of $\text{LiTi}_2(\text{PO}_4)_3$. This can be explained by the fact that some of the Ti^{4+} was transformed to

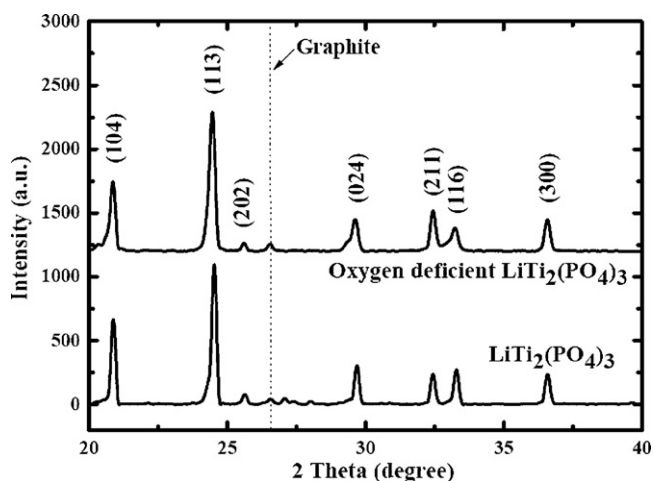


Fig. 2. XRD patterns of the $\text{LiTi}_2(\text{PO}_4)_3$ sample heat treated under air and the oxygen deficient $\text{LiTi}_2(\text{PO}_4)_3$ sample under N_2 .

Ti^{3+} in the oxygen deficient $\text{LiTi}_2(\text{PO}_4)_3$ heat treated under N_2 , and the Ti^{3+} ion is larger in size (0.81 Å) compared to the Ti^{4+} ion (0.75 Å) [42].

The core-level XPS spectra of O, Ti and P measured on the surface of the $\text{LiTi}_2(\text{PO}_4)_3$ sample heat treated under air and the oxygen deficient $\text{LiTi}_2(\text{PO}_4)_3$ sample under N_2 are shown in Fig. 3. To exclude any effects on the values of binding energies due to charging of the samples during the XPS analysis, all data were corrected by a linear shift such that the peak maximum of the C 1s binding energy of adventitious carbon corresponded to 284.6 eV. The XPS spectra of the O 1s region was composed of many peaks, corresponding to the O in Li–O, Ti–O–P and P=O bonds [45–47]. The Ti 2p peaks include 464.6 and 458.8 eV, indicating that the Ti ions are in an octahedral environment [45]. The P 2p signals at 133.5 eV for $\text{LiTi}_2(\text{PO}_4)_3$ and 133.6 eV for oxygen deficient $\text{LiTi}_2(\text{PO}_4)_3$ are identified as being in the pentavalent oxidation state (P^{5+}) [45,48]. There is no indication of the Ti–P bond due to the absence of the characteristic peak at 128.6 eV [49].

Fig. 4 shows the highly resolved Ti $2p_{3/2}$ XPS peak and its fitted Gaussian peaks. An obvious change occurred in the Ti $2p_{3/2}$ spectrum for the oxygen deficient $\text{LiTi}_2(\text{PO}_4)_3$ sample heat treated under N_2 . De-summation of the spectrum resulted in the foundation of the peak belonging to Ti ion with low valence, Ti^{3+} , which is Ti $2p_{3/2}$ located at 457.6 eV [50–52]. In detail, Ti^{3+} was detected in the oxygen deficient $\text{LiTi}_2(\text{PO}_4)_3$ sample heat treated under N_2 , while the Ti $2p_{3/2}$ signal of the $\text{LiTi}_2(\text{PO}_4)_3$ sample heat treated under

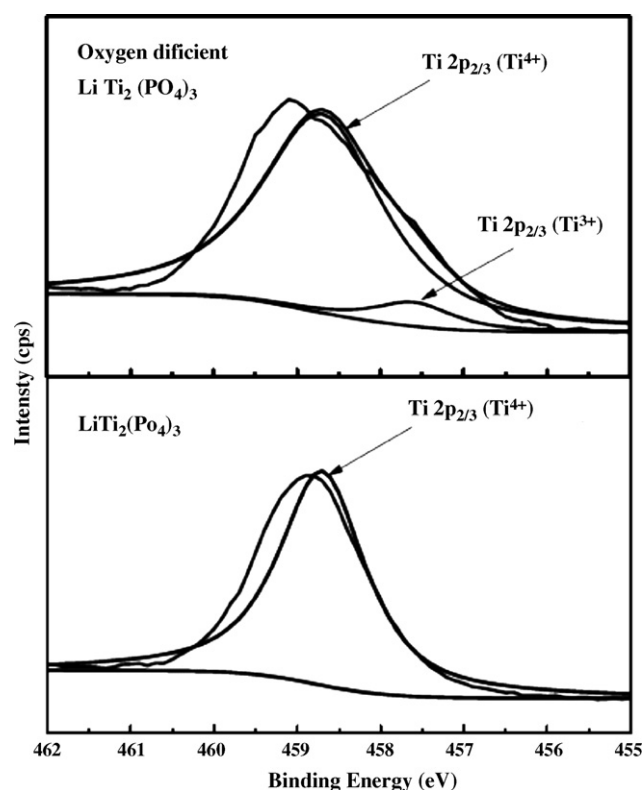


Fig. 4. Ti $2p_{3/2}$ XPS spectra of the $\text{LiTi}_2(\text{PO}_4)_3$ sample heat treated under air and the oxygen deficient $\text{LiTi}_2(\text{PO}_4)_3$ sample under N_2 .

air belonged to Ti^{4+} only. We assume that after heat treatment under poor oxygen conditions, the oxygen vacancy defects could be formed in $\text{LiTi}_2(\text{PO}_4)_3$, resulting in the presence of the mixed $\text{Ti}^{4+}/\text{Ti}^{3+}$ valence, which can explain the darker color and increased lattice parameter of the oxygen deficient $\text{LiTi}_2(\text{PO}_4)_3$ sample compared to the air sample, where only Ti^{4+} is present. However, the exact amount of vacancy oxygen in oxygen deficient $\text{LiTi}_2(\text{PO}_4)_3$ could not be derived, because we cannot detect the exact materials for their slight amount. What we know is that they should be $\text{LiTi}_2(\text{PO}_{4-x})_3$ or other impurities containing lower valence Ti.

It was expected that oxygen deficient $\text{LiTi}_2(\text{PO}_4)_3$ would exhibit a higher electronic conductivity than $\text{LiTi}_2(\text{PO}_4)_3$ as a result of the mixed $\text{Ti}^{4+}/\text{Ti}^{3+}$ valence, which would lead to increased number of electrons and hence a higher electronic conductivity. As for the oxygen deficient $\text{LiTi}_2(\text{PO}_4)_3$, the electronic conductivity was increased

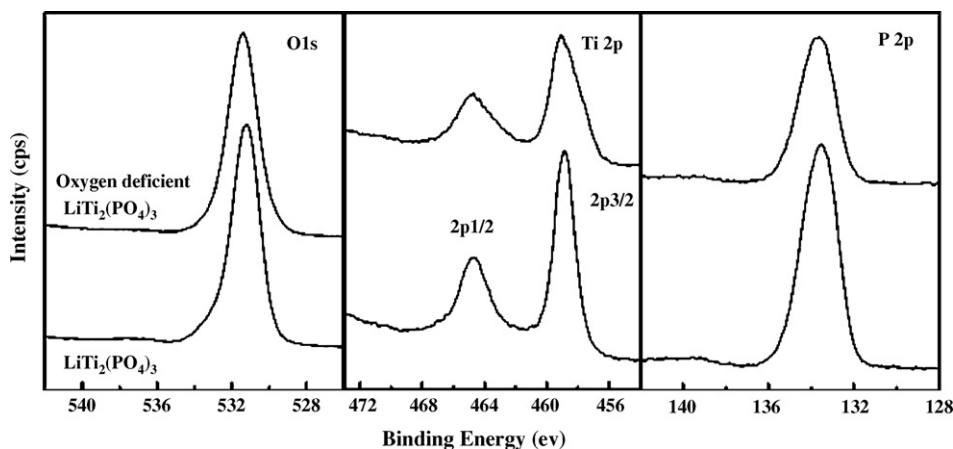


Fig. 3. O 1s, Ti 2p, and P 2p XPS spectra of the $\text{LiTi}_2(\text{PO}_4)_3$ sample heat treated under air and the oxygen deficient $\text{LiTi}_2(\text{PO}_4)_3$ sample under N_2 .

Table 1
Electrical conductivity of $\text{LiTi}_2(\text{PO}_4)_3$ and oxygen deficient $\text{LiTi}_2(\text{PO}_{4-x})_3$.

	Conductivity (S cm)
$\text{LiTi}_2(\text{PO}_4)_3$	$4.4\text{E}-8$
Oxygen deficient $\text{LiTi}_2(\text{PO}_{4-x})_3$	$1.7\text{E}-6$

nearly two orders of magnitude compared to that of $\text{LiTi}_2(\text{PO}_4)_3$ due to the presence of the mixed $\text{Ti}^{4+}/\text{Ti}^{3+}$ valence, as shown in Table 1. It should be noted that the absolute values in Table 1 may not reflect the precise electronic conductivity for the $\text{LiTi}_2(\text{PO}_4)_3$ samples due to our experimental set-up and conditions. However, the relatively higher electronic conductivity would lead oxygen deficient $\text{LiTi}_2(\text{PO}_4)_3$ to exhibit a better rate capability.

Typical charge/discharge curves for the $\text{LiTi}_2(\text{PO}_4)_3$ and oxygen deficient $\text{LiTi}_2(\text{PO}_4)_3$ samples are shown in Fig. 5. The cells were cycled between 1.5 and 3.5 V at 28 mA g^{-1} (0.2 C), 70 mA g^{-1} (0.5 C) and 140 mA g^{-1} (1.0 C) at room temperature. Both electrodes delivered a discharge capacity of about 118 mAh g^{-1} with a voltage plateau of 2.45 V at 28 mA g^{-1} , which indicated a two phase mechanism for lithium insertion. When the charge/discharge rates were increased to 1 C, oxygen deficient $\text{LiTi}_2(\text{PO}_4)_3$ could present a discharge capacity of 93 mAh g^{-1} , compared to 81 mAh g^{-1} for $\text{LiTi}_2(\text{PO}_4)_3$.

The discharge capacities as a function of rate for the $\text{LiTi}_2(\text{PO}_4)_3$ and oxygen deficient $\text{LiTi}_2(\text{PO}_4)_3$ samples are shown in Fig. 6. We can see that both samples had a decrease in capacity as a function of the rate. However, the capacity for oxygen deficient $\text{LiTi}_2(\text{PO}_4)_3$ at rates greater than 0.5 C is clearly higher than that for $\text{LiTi}_2(\text{PO}_4)_3$, and the difference increases with greater rates. This result is expected because of the higher electronic conductivity of $\text{LiTi}_2(\text{PO}_{4-x})_3$ compared to $\text{LiTi}_2(\text{PO}_4)_3$ as a result of the mixed $\text{Ti}^{4+}/\text{Ti}^{3+}$ valence.

To further confirm the possibility whether oxygen vacancy could be formed in $\text{LiTi}_2(\text{PO}_4)_3$ under O-poor conditions, investigate the

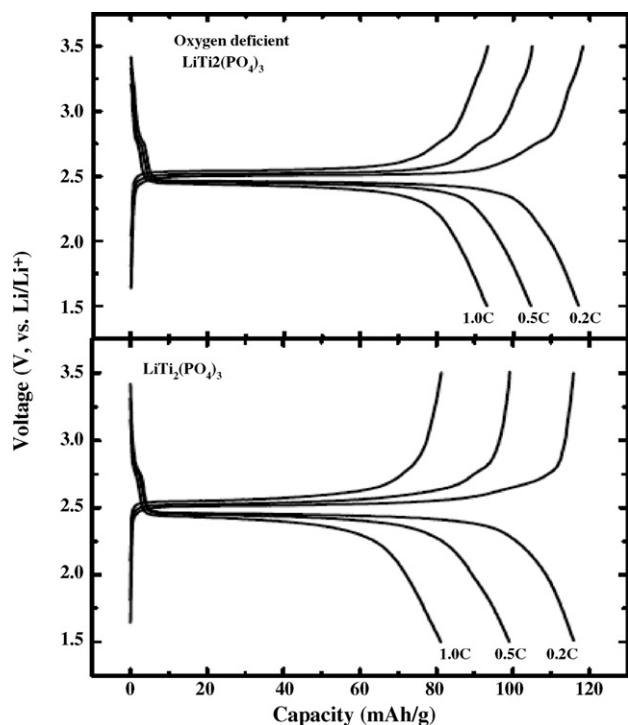


Fig. 5. Typical charge/discharge curves for (A) oxygen deficient $\text{LiTi}_2(\text{PO}_4)_3$ and (B) $\text{LiTi}_2(\text{PO}_4)_3$ cycled between 1.5 and 3.5 V at 0.2, 0.5, and 1.0 C at room temperature.

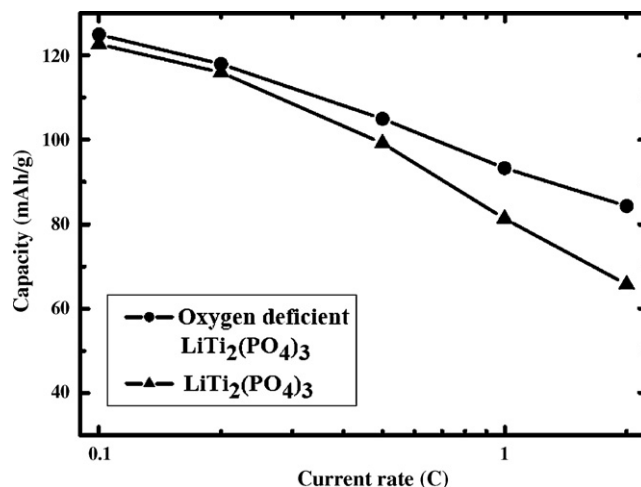


Fig. 6. Discharge capacity as a function of rate for oxygen deficient $\text{LiTi}_2(\text{PO}_4)_3$ and $\text{LiTi}_2(\text{PO}_4)_3$ cycled between 1.5 and 3.5 V at room temperature.

impact of oxygen vacancies on the electronic conductivity of the $\text{LiTi}_2(\text{PO}_4)_3$, we used the first-principles to calculate the formation energy of an oxygen vacancy and electronic densities of states in $\text{LiTi}_2(\text{PO}_4)_3$.

The unit cell of $\text{LiTi}_2(\text{PO}_4)_3$ contains four formula units. From the point of view of symmetry, all the Li, Ti and P atoms are equivalent in $\text{LiTi}_2(\text{PO}_4)_3$, but there are two types of O atoms, as shown in Fig. 7. The optimized lattice constants for $\text{LiTi}_2(\text{PO}_4)_3$ are listed in Table 2 along with the experimental values. Our theoretical results are in excellent agreement with the experimental data, with less than 1.4% error for the lattice volume.

The formation energy of an oxygen vacancy is dependent upon the oxygen partial pressure and the temperature during sample

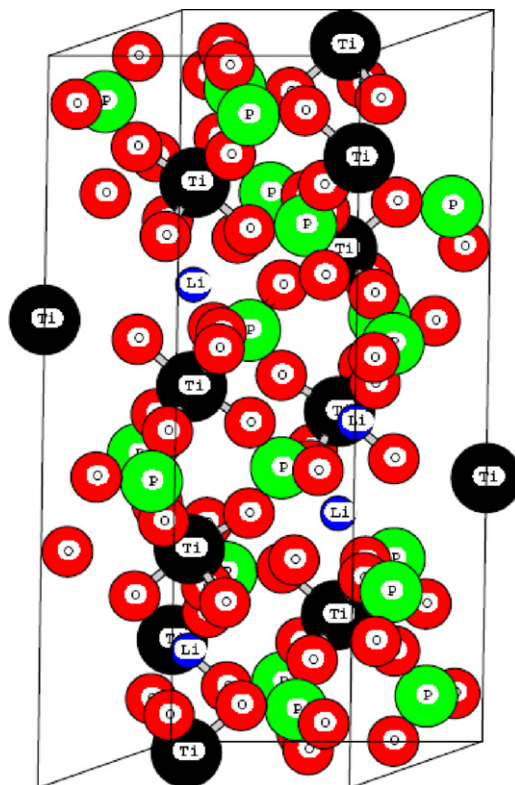


Fig. 7. The crystal structure of $\text{LiTi}_2(\text{PO}_4)_3$.

Table 2
Calculated and experimental lattice parameters for $\text{LiTi}_2(\text{PO}_4)_3$.

	a (Å)	b (Å)	c (Å)	Volume (Å ³)
$\text{LiTi}_2(\text{PO}_4)_3$ (Calc.)	8.534	8.534	20.457	1290.32
$\text{LiTi}_2(\text{PO}_4)_3$ (Expt.) [53]	8.511	8.511	20.843	1307.53

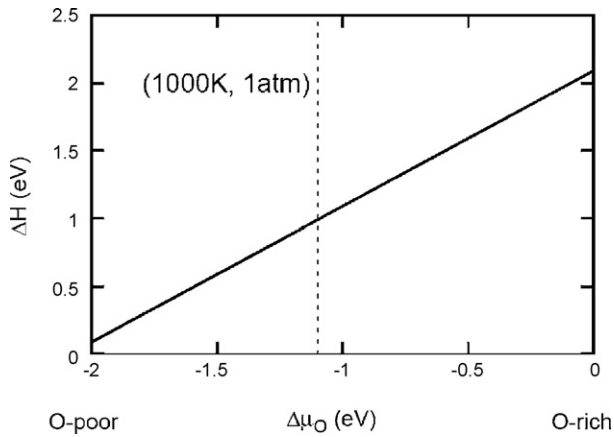


Fig. 8. The formation energy of oxygen vacancies at various oxygen chemical potentials. The dashed line corresponds to the O chemical potential at 1000 K with O partial pressure of 1 atm.

preparation. The chemical potential of oxygen may be described by [54]:

$$\mu_{\text{O}}(T, p) = \mu_{\text{O}}(T, p^0) + \frac{1}{2} kT \ln(p/p^0)$$

The oxygen vacancy was found to be a 2^+ positive charge under most conditions [25,35,43]. The dependence of the oxygen vacancy formation energy on the oxygen chemical potential is shown in

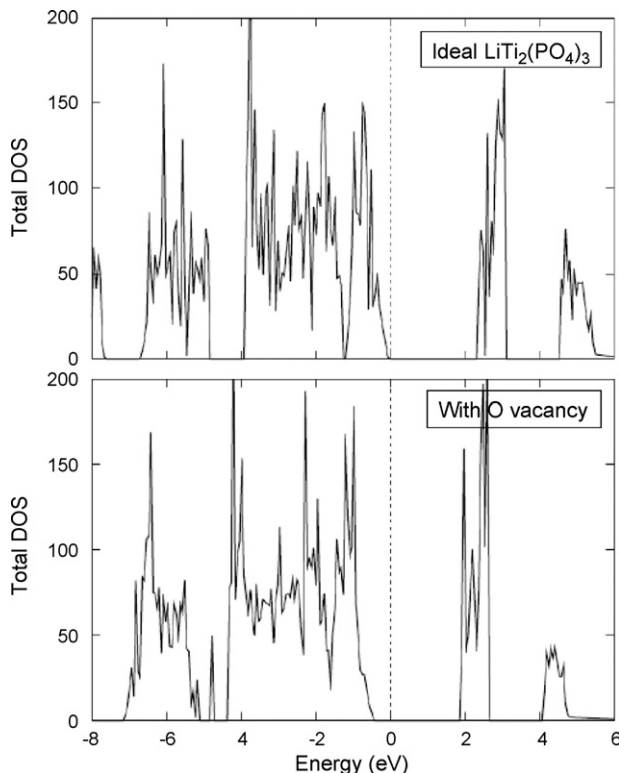


Fig. 9. Total DOS of $\text{LiTi}_2(\text{PO}_4)_3$ with and without oxygen vacancies.

Fig. 8. Under the O-rich conditions, $\Delta\mu_{\text{O}}$ is set to zero and $\mu_{\text{O}}^{\text{Solid}} = \frac{1}{2} E_{\text{O}_2}^{\text{total}} = \mu_{\text{O}}(\text{OK}, p^0)$. The oxygen chemical potential at 1000 K with an oxygen partial potential of 1 atm is also denoted by a dashed line in Fig. 8. It is clear that under O-rich conditions, the formation energy of an oxygen vacancy is as high as 2.09 eV, indicating that an oxygen vacancy is difficult to form in $\text{LiTi}_2(\text{PO}_4)_3$. However, as the oxygen partial pressure decreases or the temperature during sample preparation increases (i.e., the oxygen chemical potential decreases), the formation energy can decrease significantly. Therefore, the oxygen vacancy can be formed in $\text{LiTi}_2(\text{PO}_4)_3$ under O-poor conditions, as in most of the metal oxides.

To further investigate the impact of oxygen vacancies on the electronic conductivity of the $\text{LiTi}_2(\text{PO}_4)_3$ sample, the electronic densities of states for $\text{LiTi}_2(\text{PO}_4)_3$ with and without oxygen vacancies are shown in Fig. 9. Obviously, the oxygen vacancies form a defect band, which decreases the energy gap of $\text{LiTi}_2(\text{PO}_4)_3$. The change of band gap due to the formation of oxygen vacancies may not increase the electronic mobility by itself. However, it may significantly decrease the donor levels of other possible donor defects and thus improve the electronic mobility.

4. Conclusion

In the present work, we found that $\text{LiTi}_2(\text{PO}_4)_3$ heat treated under a N_2 atmosphere shows increased electronic conductivity, nearly two orders of magnitude compared to that of $\text{LiTi}_2(\text{PO}_4)_3$. This increase in electronic conductivity is due largely to the oxygen vacancies in oxygen deficient $\text{LiTi}_2(\text{PO}_4)_3$. The presence of a mixed $\text{Ti}^{4+}/\text{Ti}^{3+}$ valence plays a large role in controlling the structure and electronic states in oxygen deficient $\text{LiTi}_2(\text{PO}_4)_3$, which then impact the electrochemical performance. First-principles calculations also suggest that the oxygen vacancies could be formed in $\text{LiTi}_2(\text{PO}_4)_3$ under oxygen-poor conditions, and this may significantly decrease the donor levels of other possible donor defects and thus improve the electronic mobility. As a result, the oxygen deficient $\text{LiTi}_2(\text{PO}_4)_3$ shows a much better rate capability as a cathode material for lithium-ion batteries compared to stoichiometric $\text{LiTi}_2(\text{PO}_4)_3$.

While we have focused on the properties of $\text{LiTi}_2(\text{PO}_4)_3$ in this work, the results have wider implications for other related materials, because they suggest that similar oxygen vacancies can occur if certain conditions are met. Therefore, the study of element stoichiometry is very important in further characterizing Mn, Ti and Fe-based electrode materials as well as in developing new electrode materials for lithium-ion batteries.

Acknowledgments

This work was partially supported by the National Natural Science Foundation of China (No. 20633040), the 863 program (No. 2006AA05Z218) and the State Key Basic Research Program of PRC (2007CB209703) and Shanghai Science & Technology Committee (08DZ2270500, 0852nm00100). J.Y. Luo acknowledges the support of Fudan Graduate Innovation Funds.

References

- [1] M.S. Whittingham, Chem. Rev. 104 (2004) 4271.
- [2] B. Scrosati, Nature 373 (1995) 557.
- [3] R.F. Nelson, J. Power Sources 92 (2001) 2.
- [4] J.Y. Luo, J.J. Zhang, Y.Y. Xia, Chem. Mater. 18 (2006) 5618.
- [5] J.Y. Luo, Y.G. Wang, H.M. Xiong, Y.Y. Xia, Chem. Mater. 19 (2007) 4791.
- [6] A.K. Padhi, K.S. Nanjundaswamy, J.B. Goodenough, J. Electrochem. Soc. 144 (1997) 1188.
- [7] A.K. Padhi, Ph.D. Thesis, the University of Texas at Austin, 1997.
- [8] A.K. Padhi, K.S. Nanjundaswamy, C. Masquelier, J.B. Goodenough, J. Electrochem. Soc. 144 (1997) 2581.

- [9] A.K. Padhi, K.S. Nanjundaswamy, C. Masquelier, S. Okada, J.B. Goodenough, J. Electrochem. Soc. 144 (1997) 1609.
- [10] K.S. Nanjundaswamy, A.K. Padhi, J.B. Goodenough, S. Okada, H. Ohtsuka, H. Arai, Yamaki, J. Solid State Ionics 92 (1996) 1.
- [11] H. Li, X. Wu, L.Q. Chen, X.J. Huang, Solid State Ionics 149 (2003) 185.
- [12] H. Li, L.H. Shi, W. Lu, X.J. Huang, L.Q. Chen, J. Electrochem. Soc. 148 (2001) A915.
- [13] S.S. Zhang, M.S. Ding, K. Xu, J. Jow, T.R. Allen, Electrochem. Solid-State Lett. 4 (2001) A206.
- [14] H. Li, L.H. Shi, Q. Wang, L.Q. Chen, X.J. Huang, Solid State Ionics 148 (2002) 247.
- [15] T. Doi, Y. Iriyama, T. Abe, Z. Ogumi, Chem. Mater. 17 (2005) 1580.
- [16] M. Wagemaker, W.J.H. Borghols, E.R.H. van Eck, A.P.M. Kentgens, G.J. Kearley, F.M. Mulder, Chem. Eur. J. 13 (2007) 2023.
- [17] J.Y. Luo, X.L. Li, Y.Y. Xia, Electrochim. Acta 52 (2007) 4525.
- [18] J.Y. Luo, L. Cheng, Y.Y. Xia, Electrochem. Commun. 9 (2007) 1404.
- [19] J.Y. Luo, H.M. Xiong, Y.Y. Xia, J. Phys. Chem. C 112 (2008) 12051.
- [20] R. Dominko, M. Bele, M. Gaberscek, M. Remskar, D. Hanzel, S. Pejovnik, J. Jamnik, J. Electrochem. Soc. 152 (2005) A607.
- [21] N. Ravet, J.B. Goodenough, S. Besner, M. Simoneau, P. Hovington, M. Armand, Abstracts of the ECS Fall Meeting Honolulu, Hawaii, October (1999), Electrochemical Society, Pennington, NJ, 1999 (Abstr. 127).
- [22] H. Huang, S.C. Yin, L.F. Nazar, Electrochem. Solid-State Lett. 4 (2001) A170.
- [23] M. Morcrette, C. Wurm, J. Gaubicher, C. Masquelier, in: C. Delmas (Ed.), Abstracts of the Lithium Battery Discussion Meeting (LiBD 2001), Arcachon, France, 2001 (Abstr. 98).
- [24] J.Y. Luo, Y.Y. Xia, Adv. Funct. Mater. 17 (2007) 3877.
- [25] S. Patoux, C. Masquelier, Chem. Mater. 14 (2002) 5057.
- [26] L. Cheng, X.L. Li, H.J. Liu, H.M. Xiong, P.W. Zhang, Y.Y. Xia, J. Electrochem. Soc. 154 (2007) A692.
- [27] Y.H. Huang, K.S. Park, J.B. Goodenough, J. Electrochem. Soc. 153 (2006) A2282.
- [28] K. Zaghib, A. Mauger, F. Gendron, C.M. Julien, Chem. Mater. 20 (2008) 462.
- [29] H.M. Xie, R.S. Wang, J.R. Ying, L.Y. Zhang, A.F. Jalbout, H.Y. Yu, G.L. Yang, X.M. Pan, Z.M. Su, Adv. Mater. 18 (2006) 2609.
- [30] H. Gabsisch, J.D. Wilcox, M.M. Doeff, Electrochem. Solid State Lett. 7 (2006) A360.
- [31] Z.H. Chen, J.R. Dahn, J. Electrochem. Soc. 149 (2002) A1184.
- [32] N. Ohta, K. Takada, L.Q. Zhang, R.Z. Ma, M. Osada, T. Sasaki, Adv. Mater. 18 (2006) 2226.
- [33] S.Y. Chung, J.T. Bloking, Y.M. Chiang, Nat. Mater. 1 (2002) 123.
- [34] P.S. Herle, B. Ellis, N. Coombs, L.F. Nazar, Nat. Mater. 3 (2004) 147.
- [35] A. Aatiq, M. Menetrier, L. Croguennee, E. Suard, C. Delmas, J. Mater. Chem. 12 (2002) 2971.
- [36] S. Sharma, L. Fransson, E. Sjostedt, L. Nordstrom, B. Johansson, K.J. Edstrom, Electrochem. Soc. 150 (2003) A330.
- [37] M.K. Aydinol, G. Ceder, J. Electrochem. Soc. 144 (1997) 3832.
- [38] G. Ceder, Y.M. Chiang, D.R. Sadoway, M.K. Aydinol, Y.I. Jang, B. Huang, Nature (London) 392 (1998) 694.
- [39] J.P. Perdew, Y. Wang, Phys. Rev. B 45 (1992) 13244.
- [40] G. Kresse, Hafner, J. Phys. Rev. B 47 (1993) 558.
- [41] G. Kresse, Furthmuller, J. Phys. Rev. B 54 (1996) 11169.
- [42] S.B. Zhang, J.E. Northrup, Phys. Rev. Lett. 67 (1991) 2339.
- [43] C.M. Burba, R. Frech, Solid State Ionics 177 (2006) 1489.
- [44] J. Wolfenstine, U. Lee, J.L. Allen, J. Power Sources 154 (2006) 287.
- [45] J.C. Yu, L.Z. Zhang, Z. Zheng, J.C. Zhao, Chem. Mater. 15 (2003) 2280.
- [46] Q.F. Wang, L. Zhong, J.Q. Sun, J.C. Shen, Chem. Mater. 17 (2005) 3563.
- [47] H.L. Fei, X.Q. Zhou, H.J. Zhou, Z.R. Shen, P.C. Sun, Z.Y. Yuan, T.H. Chen, Micropor. Mesopor. Mater. 100 (2007) 139.
- [48] T.Z. Ren, Z.Y. Yuan, A. Azoune, J.J. Pireaux, B.L. Su, Langmuir 22 (2006) 3886.
- [49] S. Baunack, S. Oswald, D. Scharnweber, Surf. Interface Anal. 26 (1998) 471.
- [50] C. Trapalis, V. Kozhukharov, B. Samunova, J. Mater. Sci. 28 (1993) 1276.
- [51] S.Z. Chen, P.Y. Zhang, W.P. Zhu, L. Chen, S.M. Xu, Appl. Surf. Sci. 252 (2006) 7532.
- [52] S. Huang, Z. Wen, X. Zhu, X. Yang, J. Electrochem. Soc. 152 (2005) A1301.
- [53] C. Delma, A. Nadiri, Mater. Res. Bull. 23 (1988) 65.
- [54] K. Reuter, M. Scheffler, Phys. Rev. B 65 (2001) 035406.